Monopole flux state on the pyrochlore lattice

F. J. Burnell
Department of Physics, Princeton University, Princeton, New Jersey 08544, USA

Shoibal Chakravarty
Princeton Environmental Institute, Princeton University, Princeton, New Jersey 08544, USA
and Department of Physics, Princeton University, Princeton, New Jersey 08544, USA

S. L. Sondhi
Princeton Center for Theoretical Science, Princeton University, Princeton, New Jersey 08544, USA
and Department of Physics, Princeton University, Princeton, New Jersey 08544, USA

(Received 17 September 2008; revised manuscript received 3 February 2009; published 28 April 2009)

The ground state of a spin-$\frac{1}{2}$ nearest-neighbor quantum Heisenberg antiferromagnet on the pyrochlore lattice is investigated using a large N SU(N) fermionic mean-field theory. We find several mean-field states, of which the state of lowest energy upon Gutzwiller projection is a parity and time-reversal breaking chiral phase with a unit monopole flux exiting each tetrahedron. This "monopole flux" state has a Fermi surface consisting of four lines intersecting at a point. At mean field the low-energy excitations about the Fermi surface are gapless spinons. An analysis using the projective symmetry group of this state suggests that the state is stable to small fluctuations which neither induce a gap nor alter the unusual Fermi surface.

DOI: 10.1103/PhysRevB.79.144432 PACS number(s): 75.10.Jm, 71.10.−w

I. INTRODUCTION

This paper lies at the intersection of two streams of research in contemporary quantum magnetism—the study of spin liquids and the study of geometrically frustrated magnetism. Specifically, we are interested in $S=1/2$ Heisenberg models on the pyrochlore lattice and were motivated by asking whether they support a zero-temperature phase that breaks no symmetries of the problem—a fully symmetric quantum spin liquid.

The study of quantum spin liquids—being defined broadly as states of spin systems that do not exhibit long-range Neél order down to zero temperature—is currently in the midst of a significant revival. The subject itself is decades old with its contemporary study tracing its origins to Anderson's introduction of the resonating valence bond (RVB) state[1] and then to his suggestion,[2] upon the discovery of the cuprate superconductors, that their behavior was traceable to a parent spin-liquid state. But its current vogue has much to do with recent progress in constructing actual models that realize spin-liquid behavior[41] and the recognition that a large class of spin liquids exemplify ordering beyond the broken-symmetry paradigm—they give rise to low-energy gauge fields but not order parameters. That such "topological phases"[42] also underlie a fascinating approach to quantum computation[3] only multiplies their interest.

The study of geometrically frustrated magnets[4] has intertwined roots. Indeed, Anderson's 1972 paper identified a small value of the spin and geometric frustration as two sources of quantum fluctuations that could favor a spin liquid. In recent years there has been steady progress in both understanding the behavior of many geometrically frustrated magnets but, more importantly, in synthesizing an increasing number of compounds that realize challenging idealizations to increasing accuracy,[5,6] leading to a resurgence of interest in these systems as well.

The pyrochlore lattice is a natural object of study in this context. It is highly frustrated and frequently realized as a sublattice of the spinels or the pyrochlores. Potentially, it could host a spin liquid in $d=3$ for small values of the spin. Much work has gone into studying its magnetic properties in various contexts. Most notably, it is known to lack long-range order with nearest-neighbor interacting classical spins,[7] but instead to exhibit an emergent gauge field and dipolar correlations as $T\rightarrow 0$. [Interestingly, this physics is realized in the Ising "spin ice" systems (Dy and Ho titanate)[8] although with an additional fundamental dipolar interaction that leads to further elegant physics involving magnetic monopoles.[9]] Attempts to work about the classical limit in the spin-wave $(1/S)$ expansion have lead to some insight into the quantum "order by disorder" selection mechanism in this limit. Though the fate of the $1/S$ expansion is not settled,[10] there is little reason to think that it can be informative when it comes to small values of spin, especially the $S=1/2$ case[43] that is our concern in this paper. This is so partly because the selection mechanism at large S is weak and leads to somewhat ornate states but also for the well-understood reason that it misses out on tunneling processes that are sensitive to the Berry phases entering the exact path integral.[11,12]

Consequently, various authors have attempted to directly tackle the $S=1/2$ problem. Harris, Berlinsky, and Bruder (HBB) (Ref. 13) initiated a cluster treatment in which the pyrochlore lattice is first decoupled into, say, its up tetrahedra and then perturbatively reconnected. Subsequently Tsunetsugu[14] worked out a more complete treatment along the same lines and found a dimerized state with a four-sublattice structure. The criticism that this work predicts symmetry breaking that is put in at the first step has attracted a potential rebuttal in the work of Berg *et al.*[15] with the "Contractor Renormalization" or CORE technique. An alternative perspective on this physics was provided in Ref. 16 where it was shown that an SU(N) deformation produces a

quantum dimer model whose physics is very reminiscent of the HBB scenario. Unfortunately, the $N=2$ limit is manifestly problematic so it has not been possible to declare victory in this work. Yet another attack on the problem[17] used an alternative large-N theory—equivalent to Schwinger boson mean-field (MF) theory —and found a delicate energetics at small values of spin (or boson density) which nevertheless strongly indicated that the spin 1/2 problem must break *some* symmetry.[44]

With this set of predictions of symmetry breaking as background, in the present work we bring another approximate large-N technique—that of "slave fermions"[18,19]—to bear on the pyrochlore problem with a view to examining whether it produces a symmetric, spin liquid, alternative. To this end we enumerate various translationally invariant mean-field solutions of which the lowest energy nondimerized solution is one we call a "monopole flux" state; upon Gutzwiller projection it also improves upon the fully dimerized states. While this state does not break lattice symmetries in the manner of the HBB scenario, it is not a spin liquid in the sense of breaking no symmetries at all. Instead it is a chiral spin liquid[20,21] and breaks parity (P) and time-reversal (T) symmetries. It also exhibits spinons in its mean-field spectrum. We describe the unusual mean-field spectrum—which yields a Fermi surface consisting of four lines intersecting at a point—and its low-energy limit in some detail. This state was first reported in Ref. 22. Subsequently it sparked a larger investigation by R. Shankar and two of us[23] on flux Hamiltonians on root lattices of Lie groups with minuscule decorations, and these results were announced there previously. The stability of the mean-field structure to fluctuations is the next question of interest. We make progress in that direction by enumerating the projective symmetry group (PSG) (Ref. 24) of the state and showing that it forbids any terms that would destabilize the mean-field Fermi surface. This still leaves the fate of the gauge fluctuations open as a matter of dynamics and we expect to discuss this elsewhere.[25] Finally we note that as we were finalizing this paper there appeared an independent evaluation of energies for Gutzwiller projected wave functions on the pyrochlore,[26] which agrees with our results on that score.

And now to the organization of the paper. We begin with a brief overview of the large-N/mean-field slave fermion treatment of the Heisenberg model in Sec. II. In Sec. III we apply this technique to generate several mean field Ansätze on the pyrochlore lattice. We identify the lowest energy state, or monopole flux state, and discuss its interesting properties. Section IV reviews in general terms how the PSG protects a mean-field state against developing symmetry-breaking terms. The PSG derived arguments for the stability of the monopole flux state are given in Sec. V, where we derive the general form of the symmetry permitted perturbations to the Hamiltonian. We conclude in Sec. VI. Details of the PSG for the monopole flux state can be found in Appendix B, while Appendix A explains the numerical technique used to carry out Gutzwiller projection.

II. LARGE-N HEISENBERG MODEL: SPINONS AND GAUGE FIELDS

In this section we briefly review the large-N fermionic approach to the $S=1/2$ SU(2) Heisenberg model, which began as a mean-field theory introduced by Baskaran *et al.*[18] and was shortly thereafter systematized via a generalization to SU(N) by Affleck and Marston.[19]

In this approach, we first replace the bosonic spin operators of the Heisenberg Hamiltonian

$$H = J\sum_{\langle ij\rangle} \mathbf{S}_i \cdot \mathbf{S}_\mathbf{j} \tag{1}$$

with bilinears in fermionic "spinon" operators,

$$\mathbf{S}_i = \frac{1}{2}\sum_{\alpha,\beta} c^\dagger_{i\alpha}\sigma_{\alpha\beta}c_{i\beta}. \tag{2}$$

The resulting Hamiltonian conserves the number of fermions at each site, and the starting spin Hamiltonian is recovered if we limit ourselves to physical states with exactly 1 particle per site. Up to a constant in the subspace of physical states, it can be rewritten in the suggestive form

$$H = -\frac{J}{2}\sum_{\langle ij\rangle}\sum_{\alpha}\sum_{\beta} c^\dagger_{i\alpha}c_{j\alpha}c^\dagger_{j\beta}c_{i\beta}. \tag{3}$$

A mean-field theory arises upon performing the Hubbard-Stratonovich decoupling

$$H = -\sum_{\alpha}\sum_{\langle ij\rangle}(c^\dagger_{i\alpha}c_{j\alpha}\chi_{ij} + \text{h.c.}) + \frac{2}{J}\sum_{\langle ij\rangle}|\chi_{ij}|^2 \tag{4}$$

and locally minimizing the classical field χ_{ij} to obtain self-consistency.

In order to understand the nature of fluctuations about such mean-field solutions it is conceptually convenient to consider the path integral defined by the equivalent Lagrangian

$$L = \sum_{i,\alpha} c^\dagger_{i,\alpha}(i\partial_t + \mu)c_{i,\alpha} + \sum_{i,\alpha}\phi_i(c^\dagger_{i,\alpha}c_{i,\alpha} - 1) + \sum_{\langle ij\rangle}\left[\sum_{\alpha}(c^\dagger_{i\alpha}c_{j\alpha}\chi_{ij} + \text{h.c.}) - \frac{2}{J}|\chi_{ij}|^2\right], \tag{5}$$

where ϕ is a Lagrange multiplier field enforcing the single occupancy constraint $\Sigma_\alpha c^\dagger_{i\alpha}c_{i\alpha}=1$.

The above Lagrangian (5) is invariant under the local gauge transformations

$$c^\dagger_i \to c^\dagger_i e^{-i\theta_i},$$

$$\chi_{ij} \to \chi_{ij}e^{i(\theta_i-\theta_j)},$$

$$\phi \to \phi + \partial\theta/\partial t, \tag{6}$$

which arise from the local constraints in the fermionic formulation. It follows that we have reformulated the Heisenberg model as a problem of fermions that live on the sites of the original lattice coupled to a U(1) gauge field and an amplitude field (the phase and amplitude of χ_{ij}) that both live on the links of the lattice. In other words, we may write $\chi_{ij} = \rho_{ij}e^{ia_{ij}}$, where $a_{ij}\to a_{ij}+\theta_i-\theta_j$ under the gauge transformation (6). The mean-field theory consists of searching for a saddle point with frozen link fields.

As the Lagrangian (5) does not directly constrain the phase of the χ_{ij}, it describes a strongly coupled gauge theory where the assumption of a weakly fluctuating gauge field invoked in the mean-field theory is, *prima facie*, suspect. To circumvent this barrier, Affleck and Marston[19] proposed a large-N framework which introduces a weak-coupling limit for the model (5) by extending the SU(2) spin symmetry group of the Heisenberg model to SU(N) with N even. The result is a theory of many spin flavors whose coupling strength scales as $J \to J/N$. In the limit that $N \to \infty$, the corresponding mean-field theory is exact; for sufficiently large but finite N one hopes that a perturbative expansion gives accurate results. The validity of the qualitative features deduced at large N in the starting SU(2) problem is, of course, hard to establish by such considerations and requires direct numerical or experimental confirmation.

To effect the large-N generalization, we replace the two spinon operators $c_\uparrow$ and $c_\downarrow$ with N spinon operators c_α. The single occupancy constraint is now modified to

$$\sum_{\alpha=1}^{N} c_{i\alpha}^\dagger c_{i\alpha} = \frac{N}{2} \tag{7}$$

and the large-N Hamiltonian has the form

$$\begin{aligned} H &= -J/N \sum_{\alpha,\beta} \sum_{\langle ij \rangle} c_{j\alpha}^\dagger c_{i\alpha} c_{i\beta}^\dagger c_{j\beta} \\ &= -\sum_{\alpha} \sum_{\langle ij \rangle} (c_{i\alpha}^\dagger c_{j\alpha} \chi_{ij} + \text{h.c.}) + \frac{N}{J} \sum_{\langle ij \rangle} |\chi_{ij}|^2. \end{aligned} \tag{8}$$

In the infinite N limit, the action is constrained to its saddle point and the mean-field solution becomes exact. Further, to lowest order in $\frac{1}{N}$ the allowed fluctuations involve moving single spinons so that as $N \to \infty$ we need only impose the constraint (7) on average.

Away from $N=\infty$ the link fields, especially the gauge field, can fluctuate again although now with a controllably small coupling. While the fate of the coupled fermion-gauge system still needs investigation, the presence of a small parameter is a great aid in the analysis, as in the recent work on algebraic spin liquids.[27]

Finally, we note that the starting SU(2) problem is special, in that it is naturally formulated as an SU(2) gauge theory.[28,29] This can have the consequence that the $N=2$ descendant of the large-N state, if stable, may exhibit a weakly fluctuating SU(2) gauge field instead of the U(1) field that arises in the above description. We will comment on this in the context of this paper at the end.

III. MEAN-FIELD ANALYSIS

A. Saddle points of the nearest-neighbor Heisenberg model

We begin by enumerating MF states which preserve translation invariance on the pyrochlore. A mean-field solution consists of a choice of link fields which minimize the mean-field energy functional for the Lagrangian (5),

$$E(\chi) = N \left[\sum_{\langle ij \rangle} \frac{1}{J} |\chi_{ij}|^2 + \sum_{\mathbf{k}} (\varepsilon(\mathbf{k}) - \mu) \right] \tag{9}$$

where $\varepsilon(\mathbf{k})$ is the energy of a spinon of momentum $\mathbf{k}$ in the fixed background χ_{ij}, and the chemical potential μ is chosen so that the constraint of one particle per site is satisfied on average.

As discussed in Sec. I, previous work on the Heisenberg model on the pyrochlore lattice has led to ground states with broken symmetries. In this work we are particularly interested in constructing a natural state on the pyrochlore that breaks as few symmetries as possible. To this end, we begin our search with especially symmetric *Ansätze* for which $\rho_{ij} \equiv \rho$ is independent of i and j, and the flux $\Phi_\Delta = \Sigma_\Delta a_{ij}$ through each face of the tetrahedron is the same. The net flux $\Sigma_{i=1}^4 \Phi_\Delta$ through each tetrahedron must be an integer multiple of 2π since each edge borders two faces such that its net contribution to the flux is 0 (mod 2π). This gives the following three candidate spin-liquid states:

(1) Uniform: $\Phi_\Delta = 0$;

(2) π Flux: $\Phi_\Delta = \pi$;

(3) Monopole: $\Phi_\Delta = \pi/2$. Every triangular face of the tetrahedron has a $\pi/2$ outwards flux—equivalent to a monopole of strength 2π placed at the center of each tetrahedron.

At infinite N a dimerized state is always the global minimum of Eq. (9) (Ref. 30); thus we also consider

(4) Dimerized: $\chi_{ij} = \chi^0$ on a set of bonds that constitute any dimer covering of the lattice but zero otherwise.

The states (1)–(3) above are analogs of the uniform, π flux, and chiral states studied previously on the square lattice.[19,21] Of the above states, (1) and (2) break no symmetries of the problem; the third preserves lattice symmetries but breaks P and T.

The states (1) and (2) are in fact particle-hole conjugates: a particle-hole transformation maps $c_i^\dagger c_j + c_j^\dagger c_i \to -c_j^\dagger c_i - c_i^\dagger c_j$, changing the sign of χ on each bond and adding π flux to each triangular plaquette. At $N=2$ this can be effectuated by an SU(2) gauge transformation so that the states (1) and (2) describe the same state after Gutzwiller projection.

The mean-field energies of these states are listed in the first column of Table I. Consistent with Rokhsar's general considerations[30,31] the fully dimerized state is lowest energy and the monopole flux state has the lowest energy of the nondimerized states. The mean-field states with N set equal to 2 do not satisfy the single-occupancy constraint. While, in principle, perturbation theory in $1/N$ can greatly improve the wave function in this regard, this is a complex business (to which we return in Secs. IV and V) ill-suited to actual energetics. Instead, the somewhat *ad hoc* procedure of (Gutzwiller) projecting the mean-field wave function onto the Hilbert space of singly-occupied sites is typically employed to improve matters. This leads to resonances and long-range correlations that can substantially lower the mean-field ground-state energy, particularly for spin-liquid-type states.

Expectation values in the Gutzwiller projection of a state can be carried out using a Monte Carlo approach, as described in Ref. 32. A brief description of the numerical method specialized to our problem is given in Appendix A.

TABLE I. Mean-field energies for projected and unprojected ground states of the mean field *Ansätze* considered. The quoted mean-field energies are the energy of (4) plus the omitted constant $-\frac{J}{4}$ per site required to make a correspondence with (1). The states (π,π) and $(\pi/2,\pi)$ are variants of the uniform and monopole state, respectively, with flux π per hexagonal plaquette. The projected wave functions were evaluated on a lattice of $5\times5\times5$ unit cells, or 500 sites for configurations with a four-site unit cell, and 1000 sites for configurations with an eight-site unit cell.

	E_{MF} (unprojected)	E_{MF} (projected)
Uniform	$-0.3333J$	$-.3752\pm0.0004$
π Flux	$-0.3333J$	$-.3752\pm0.0004$
Monopole	$-0.3550J$	$-.4473\pm0.0009$
Dimer	$-.375J$	$-.375J$
(π,π)	$-0.3333J$	-0.3751 ± 0.0008
$(\pi/2,\pi)$	$-0.3491J$	-0.4356 ± 0.0003

The second column in Table I shows the numerically evaluated energies of the four mean-field states with Gutzwiller projection. We see that the monopole flux state now emerges as the lowest-energy state of our quartet. Encouraged by this, and also because the state has various elegant properties, we will focus in the remainder of this work on the properties of the monopole flux state. Note however, that we have failed to preserve all symmetries of the Hamiltonian even in this approach—we are forced to break T and P and thus end up with a chiral spin liquid. We give a fuller description of the symmetries of the state below.

Finally, we note that larger unit cells can be consistent with translationally invariant states.[45] Such states have an integral multiple of $\pi/2$ flux through each triangular plaquette, but also nontrivial flux through the hexagonal plaquettes in the kagomé planes, as for the mean-field states on the kagomé studied in Ref. 33. By the same arguments as employed for a single tetrahedron, we find that the flux through the hexagons must have values 0 or π (mod 2π) to preserve the translational symmetry of the lattice. (A flux of $\pi/2$ per hexagonal plaquette necessarily breaks lattice translations.) However, as noted in Table I, we find that these states also have higher energies than the monopole flux state both at mean field and upon Gutzwiller projection. The above results do not guarantee that the monopole flux state is the true ground state of the nearest-neighbor pyrochlore antiferromagnet. Indeed, numerical studies of the planar pyrochlore find energies of $-0.55J$ per unit cell for valence bond crystals for a configuration compatible with the full pyrochlore lattice,[34] and higher spin interactions may be necessary to stabilize the monopole flux state, as is the case for the π-flux state on the square lattice.[19,35] Since such terms generically exist, our focus here is on describing the energetically optimal spin-liquid state, rather than on the exact ground state of the nearest-neighbor Heisenberg antiferromagnet.

B. Monopole flux state

The monopole flux state exhibits a flux of $\pi/2$ per triangular face. To write down the mean-field Hamiltonian explicitly we must pick a gauge. We choose $\chi_{ij}=\rho_0 e^{ia_{ij}}$, with $a_{ij}=\pm\pi/2$. The phase of $\pm i$ that a spinon picks up when hopping from site i to j can be represented as an arrow on the corresponding edge, which points from i to j (j to i) if the resulting phase is $+(-)i$. The orientation of the link fields, shown in Fig. 1, gives an inward flux of $\pi/2$ per plaquette.

The necessity of picking a gauge for the mean-field solution causes, as usual, various symmetries to be implemented projectively. For example, the assignment shown in Fig. 1 is not invariant under lattice rotations. However, the background link fields after rotation can be gauge transformed to the original state, as expected from the manifestly rotation invariant assignment of fluxes. We discuss these and other symmetries in more detail in Secs. IV and V; here we merely note that P and T are the only symmetries broken by the monopole flux state.

The Hamiltonian for spinons in the gauge choice shown in Fig. 1 is

$$H=-\rho_0\sum_{\mathbf{k},\alpha}\Psi^{\dagger}_{\mathbf{k}\alpha}\begin{bmatrix} 0 & \sin\left(\frac{k_x+k_y}{4}\right) & \sin\left(\frac{k_y+k_z}{4}\right) & \sin\left(\frac{k_x+k_z}{4}\right) \\ \sin\left(\frac{k_x+k_y}{4}\right) & 0 & \sin\left(\frac{k_x-k_z}{4}\right) & \sin\left(\frac{k_z-k_y}{4}\right) \\ \sin\left(\frac{k_y+k_z}{4}\right) & \sin\left(\frac{k_x-k_z}{4}\right) & 0 & \sin\left(\frac{k_y-k_x}{4}\right) \\ \sin\left(\frac{k_x+k_z}{4}\right) & \sin\left(\frac{k_z-k_y}{4}\right) & \sin\left(\frac{k_y-k_x}{4}\right) & 0 \end{bmatrix}\Psi_{\mathbf{k}\alpha}, \tag{10}$$

where Ψ is a four-component vector, with $\Psi^i_{\mathbf{k}\alpha}=c^i_{\alpha\mathbf{k}}$. Here the index i labels the four sites in the tetrahedral unit cell.

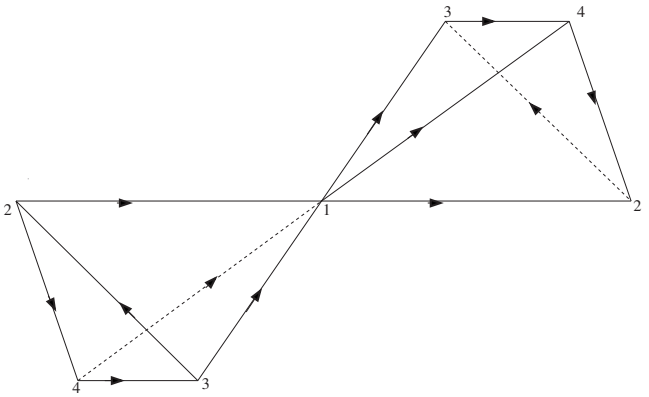

FIG. 1. Link field orientations in the monopole state with $\chi = \pm i\rho_0$. Hopping along the direction of an arrow induces a phase of $\pi/2$; hopping against the arrows, a phase of $-\pi/2$. The flux on each triangular face is $\pi/2$ inwards. With this flux assignment the monopole flux state breaks T and P, but is invariant under lattice translations and rotations.

Figure 2(b) shows a plot of the energy eigenvalues of Eq. (10) along the high-symmetry lines of the Brillouin zone. At half filling, the Fermi "surface" consists of the lines $k(\pm 1, \pm 1, \pm 1)$ which join the point (0,0,0) to the center of the hexagonal faces of the Brillouin zone of the cubic fcc lattice [line $(L-\Gamma)$ in Fig. 2(b)]. Each Fermi line has a pair of zero energy eigenstates.

Figures 3(a) and 3(b) shows a surface of constant energy $E \approx 0$ near the Fermi surface. At $E=0$, the four bands intersect only at the origin and the constant-energy surface is given by the four lines described above. Surfaces of constant energy $E \approx 0$, $E \neq 0$ consist of four cylinders enclosing the (1,1,1) directions, which are the surfaces of constant energy for particlelike $(E>0)$ or holelike $(E<0)$ excitations about the Fermi line. About the origin all four bands have energy linear in k, and another, diamond-shaped constant-energy surface appears. These surfaces intersect at the band crossings along the x, y, and z axes.[46]

C. Low-energy expansions of the spinon dispersion

The low-energy structure of the monopole flux state can be divided into two regions: R_1, the set of four Fermi lines sufficiently far from the origin, and R_0, the area near the origin.

In R_1, only two of the four bands lie near the Fermi surface, and the low-energy theory is effectively two dimensional. Linearizing the Hamiltonian about one of the Fermi lines gives

$$H[\varepsilon,\theta] = \Psi^{\dagger}_{1\alpha}[k,\varepsilon,\theta](\varepsilon \cos\theta\tau_1 + \varepsilon \sin\theta\tau_2)\Psi_{1\alpha}[k,\varepsilon,\theta], \tag{11}$$

with energies $\pm\varepsilon$, independent of θ. Here we have used the local coordinate system

$$(q_1,q_2,q_3) = \left(k + \sqrt{\frac{2}{3}}u, k - \frac{u}{\sqrt{6}} - \frac{v}{\sqrt{2}}, k - \frac{u}{\sqrt{6}} + \frac{v}{\sqrt{2}}\right), \tag{12}$$

with $\theta(u,v)=\tan^{-1}(v/u)$ and $\epsilon(u,v)=\rho_0\sqrt{u^2+v^2}/(2\sqrt{2})$. Curiously, at mean field the low-energy spectrum is independent of the position k *along* the Fermi line, depending only on the momentum component in the kagomé planes perpendicular to the vector $\boldsymbol{l}_i$. Thus the linearized theory away from the origin consists of a continuum of flavors of Dirac fermions confined to the kagomé planes orthogonal to this line.

In R_0 all four bands have energies vanishing linearly as $k \to 0$, and the low-energy Hamiltonian is given by

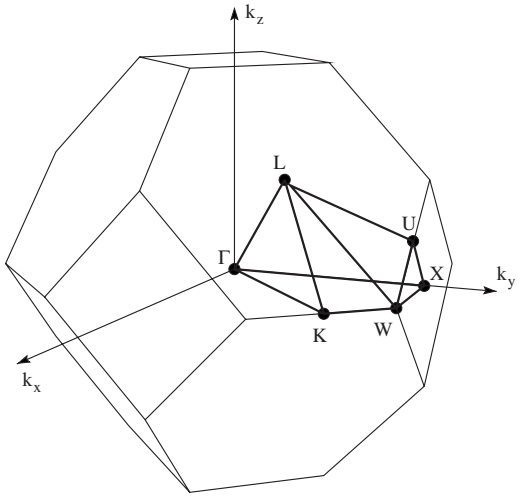

(a)

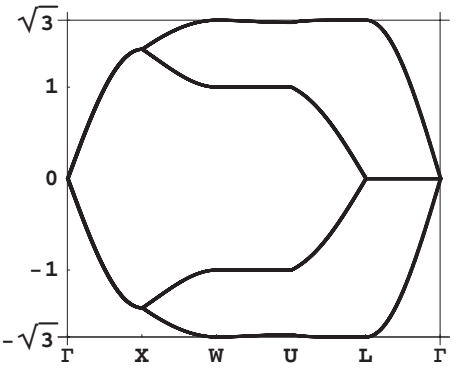

(b)

FIG. 2. Spectrum of the monopole state (a) shows the contour in the Brillouin zone along which the spectrum is plotted. (b) shows the spectrum of the monopole flux state along this high-symmetry contour in the Brillouin zone. Note the Fermi line $\frac{1}{\sqrt{3}}(k,k,k)$.

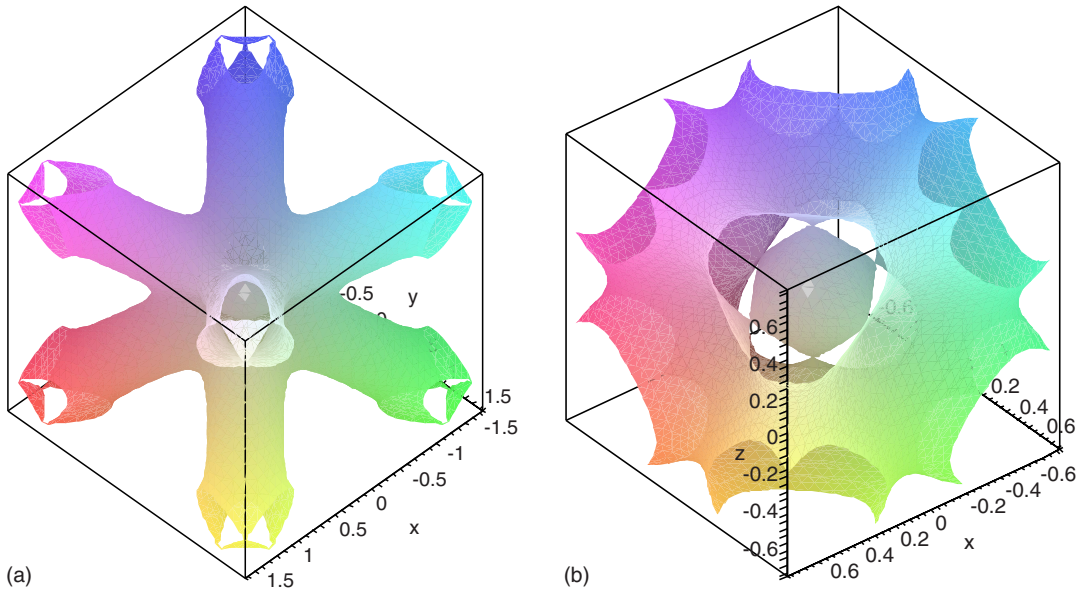

FIG. 3. (Color online) Constant energy surfaces of the monopole flux state, for $E/J=0.5$. Decreasing E/J makes the cylinders thinner. (a) A view of the cube of side length π surrounding the origin. Eight cylinders surrounding the eight Fermi lines emanate from the origin; at the origin a diamond-line shape (the low-energy spectrum of the remaining two bands) can also be seen. This shape repeats at the cube´s corners $(\pm\pi, \pm\pi)$. (b) A close-up view of the region surrounding the origin. Altering the ratio E/J shrinks the entire structure, but does not change its shape.

$$H = -\rho_0 \sum_{k,\alpha} \Psi_k^{\dagger\alpha} \begin{bmatrix} 0 & \frac{k_x+k_y}{4} & \frac{k_y+k_z}{4} & \frac{k_x+k_z}{4} \\ \frac{k_x+k_y}{4} & 0 & \frac{k_x-k_z}{4} & \frac{k_z-k_y}{4} \\ \frac{k_y+k_z}{4} & \frac{k_x-k_z}{4} & 0 & \frac{k_y-k_x}{4} \\ \frac{k_x+k_z}{4} & \frac{k_z-k_y}{4} & \frac{k_y-k_x}{4} & 0 \end{bmatrix} \Psi_{k\alpha} \tag{13}$$

with energy eigenvalues

$$\varepsilon = \pm \rho_0 \sqrt{\frac{1}{8}\sum_i k_i^2 \pm \frac{1}{8}\sqrt{3\sum_{(i<j)} k_i^2 k_j^2}}. \tag{14}$$

This dispersion relation also gives massless spinons; however, the theory is no longer one of Dirac fermions.

In addition to four bands touching at the origin, the linearized Hamiltonian (13) has two zero eigenvalues on each Fermi line. Restricting the spinors to the corresponding low-energy subspace again yields the expression (11). Thus Eq. (13) captures the principal features of the low-energy behavior not only in the vicinity of the origin, but throughout the entire Brillouin zone.

The linearized Hamiltonian has several interesting features. First, we may express it in terms of three matrices as follows:

$$H = \frac{\rho_0}{4}(\alpha_x k_x + \alpha_y k_y + \alpha_z k_z). \tag{15}$$

The α matrices are reminiscent of Dirac γ matrices, albeit with a tetrahedrally invariant, rather than rotationally invariant, algebraic structure. They do not comprise a Clifford algebra, but obey the anticommutation relations

$$\{\alpha_i, \alpha_j\} = 2\delta_{ij} + \sqrt{6}|\varepsilon_{ijk}|W_k,$$

$$\{W_i, W_j\} = 2\delta_{ij}. \tag{16}$$

Further, in a 3+1 dimensional Dirac theory there are two matrices (γ_0 and γ_5) which anticommute with all γ_i. In this sense our mean-field Hamiltonian more resembles a 2+1 dimensional Dirac theory: there is a unique matrix α_0 such that $\{\alpha_0, \alpha_i\}=0$, $i=1\ldots3$, given by

$$\alpha^{(0)} = \frac{1}{\sqrt{N}} \begin{bmatrix} 0 & \cos(k_y)\cos(k_x) & \cos(k_y)\cos(k_z) & \cos(k_x)\cos(k_z) \\ -\cos(k_y)\cos(k_x) & 0 & \cos(k_x)\cos(k_z) & -\cos(k_y)\cos(k_z) \\ -\cos(k_y)\cos(k_z) & -\cos(k_x)\cos(k_z) & 0 & \cos(k_y)\cos(k_x) \\ -\cos(k_x)\cos(k_z) & \cos(k_y)\cos(k_z) & -\cos(k_y)\cos(k_x) & 0 \end{bmatrix}, \tag{17}$$

where N is a normalization factor such that $(\alpha^{(0)})^2=1$. In the continuum limit this reduces to

$$\alpha^{(0)} = \begin{bmatrix} 0 & \frac{1}{\sqrt{3}} & \frac{1}{\sqrt{3}} & \frac{1}{\sqrt{3}} \\ \frac{-1}{\sqrt{3}} & 0 & \frac{1}{\sqrt{3}} & \frac{-1}{\sqrt{3}} \\ \frac{-1}{\sqrt{3}} & \frac{-1}{\sqrt{3}} & 0 & \frac{1}{\sqrt{3}} \\ \frac{-1}{\sqrt{3}} & \frac{1}{\sqrt{3}} & \frac{-1}{\sqrt{3}} & 0 \end{bmatrix}. \quad (18)$$

$\alpha^{(0)}$ acts as a spectrum inverting operator on H, interchanging hole states at energy $-E(k)$ with particle states at energy $E(k)$.

We point out that many of the interesting features of the low-energy spectrum of the monopole flux state can be generalized to a class of lattices whose geometry is related to certain representations of Lie groups.[23] Indeed, the four sites in the tetrahedral unit cell can be viewed as the four weights in the fundamental representation of SU(4); hopping on the pyrochlore is then analogous to acting with the appropriate raising and lowering operators. This perspective gives an explicit connection between the hopping Hamiltonian (13) and the ladder operators in the fundamental representation of SU(4). Analogous hopping problems can be studied for various other Lie group representations, as outlined in detail in Ref. 23.

To summarize, the monopole flux state is a spin liquid which preserves all symmetries of the full Hamiltonian except P and T. At mean-field level it has gapless spinons along a one-dimensional Fermi surface of four lines which intersect at the origin. Though strictly at $N=\infty$ it has higher energy than the dimerized state, Gutzwiller projection suggests that for $N=2$ this is no longer the case, and the monopole flux state is the lowest energy simple mean field *Ansatz* after projection. We now turn our attention to what can be said about the stability of this rather unusual mean-field state.

IV. STABILITY OF THE MEAN-FIELD SOLUTION: THE ROLE OF THE PSG

Next, we would like to address the question of whether the mean-field solutions described above maintain their basic properties at finite N and whether this holds all the way to $N=2$. This is a difficult problem, whose complete solution is not available even for the longer studied cases of the algebraic spin liquids in $d=2$.[47] However, following that work the general idea would be to try and understand if the state is truly stable at large enough N while leaving the question of stability at small N to detailed numerical investigation.

There are several questions here. First, is the mean-field solution locally stable? Second, is it the global minimum? Third, assuming the answer thus far is in the affirmative, is the expansion about the mean-field solution well behaved? Ideally, this would mean convergent, but it would be sufficient to know that it does not destroy the qualitative features of the gapless spinon dispersion at mean field. For example, in the case of the algebraic spin liquids in $d=2$ the spinons interact and acquire anomalous dimensions away from $N=\infty$ but they remain gapless in the vicinity of a discrete set of points.[27] Finally, what is the spectrum of collective (gauge) excitations that arise in this expansion?

Based on the experience with spin liquids in $d=2$, answering the first two questions in the affirmative is likely to require the addition of more terms to the Hamiltonian although it may be possible to choose them so that they become trivial at $N=2$.[19] We have not investigated this in detail but there does not appear to be an obstacle to doing this.

The third and fourth questions require detailed consideration of the symmetry properties and the detailed dynamics of the expansion which is that of a lattice gauge theory with matter and gauge fields in some fashion. In this work we will carry out the first part of this program which goes under the study of the "Projective Symmetry Group" (PSG) discussed in detail by Wen.[24] In this section we review the concept of the PSG and its implications for perturbative expansions. We also show explicitly how at $N=\infty$, or in mean-field theory, the PSG helps us understand the stability of particular mean-field solutions.

Turning first to the PSG, observe that although the original Hamiltonian formulated in terms of spin operators is invariant under the full space group of the pyrochlore lattice, the actual mean-field Hamiltonian of the monopole flux state is not: many of the symmetry transformations map the mean-field Hamiltonian into different *but gauge equivalent* Hamiltonians. Thus, when working in the gauge theory formulation of the problem, the actual symmetry transformations of the mean-field Hamiltonian have the form

$$c_i \to g_s[s(c_i)], \quad (19)$$

where s is an element of the space group and g is a gauge transformation. As the full Hamiltonian is gauge invariant, Eq. (19) is simply an alternative formulation of the lattice symmetries. Hence as emphasized by Ref. 24, these projective symmetry operators are exactly analogous to lattice symmetries in the original spin problem. Indeed, the correct choice of gauge transformation ensures that both H_{MF} and H are invariant under the PSG, so that the family

$$H_\lambda = H_{\mathrm{MF}} + \lambda(H - H_{\mathrm{MF}}) \quad (20)$$

is also invariant and perturbative corrections in $H-H_{\mathrm{MF}}$ cannot break the PSG symmetry.

Before discussing the implications of PSG symmetry for the monopole flux state, we would like to briefly underline how the PSG constrains the mean-field theory at infinite N, which is a much simpler but still instructive exercise.

Ignoring the dimerization instability, the monopole flux state is a mean-field minimum for nearest-neighbor couplings. The PSG is the symmetry group of the corresponding mean-field Hamiltonian. We may now ask what happens to the PSG if further neighbor couplings are included in the Hamiltonian: in particular, do they lead to terms in the new mean-field Hamiltonians that modify the PSG found earlier?

At $N=\infty$ this is a problem of minimizing the expectation value of the sum of the quadratic Hamiltonian in Eq. (4) and the new generic terms

$$\delta H = -\sum_{\alpha}\sum_{(ij)}{}'(c_{i\alpha}^{\dagger}c_{j\alpha}\chi_{ij} + \text{h.c.}) + \frac{N}{J_{ij\,(ij)}}\sum{}'|\chi_{ij}|^2, \quad (21)$$

wherein the primed sum runs over non-nearest-neighbor bonds and the J_{ij} are much smaller than the nearest-neighbor J. We will now show that, generically, the result of the new minimization for the perturbed problem preserves the PSG for the nearest-neighbor problem. While we use the language of perturbing about the monopole flux state, the argument is general.

With the addition of the perturbation, the functional that we need to minimize over the full set of $\{\chi_{ij}\}$ is

$$E_{\text{MF}} = \langle H^{(F)} + \delta H^{(F)}\rangle_{H+\delta H} + \frac{N}{J}\sum_{\langle ij\rangle}|\chi_{ij}|^2 + \frac{N}{J_{ij\,(ij)}}\sum{}'|\chi_{ij}|^2, \quad (22)$$

where the superscript (F) denotes the fermionic part of the Hamiltonian. Let $\chi_{ij}^{(0)}$ denote the values of the link fields when $\delta H \equiv 0$, i.e., in the monopole flux state. For small J_{ij} we expect the new minimum to lie not far from the old one, whence the link fields will be close to the values $\chi_{ij}^{(0)}$. Consequently we will compute the expectation value required in the above equation in perturbation theory in δH about H. (If such an expansion fails to have any radius of convergence then we are already parked at a phase transition and no stability argument is possible.)

This expansion,

$$E_{\text{MF}}(\{\chi_{ij}\}) = E_0 + \langle 0|\delta H^{(F)}|0\rangle + \sum_{n>0}\frac{|\langle 0|\delta H^{(F)}|n\rangle|^2}{E_0 - E_n} + \cdots + \frac{N}{J}\sum_{\langle ij\rangle}|\chi_{ij}|^2 + \frac{N}{J_{ij\,(ij)}}\sum{}'|\chi_{ij}|^2, \quad (23)$$

where the numerical indices refer to the ground and excited states of the unperturbed Hamiltonian $H^{(F)}(\{\chi_{ij}^{(0)}\})$, has three properties that we need. First, the linear term takes the explicit form

$$-\sum_{\alpha}\sum_{(ij)}{}'\langle c_{i\alpha}^{\dagger}c_{j\alpha}\rangle\delta\chi_{ij} + \text{h.c.} \quad (24)$$

where $\delta\chi_{ij}$ is χ_{ij} for the new bonds and the deviation from $\chi_{ij}^{(0)}$ for the nearest-neighbor bonds. This implies that new minimization likes to turn on exactly those χ_{ij} that transform as the expectation values $\langle c_{i\alpha}^{\dagger}c_{j\alpha}\rangle$. If these are, in fact, what get turned on, then the new mean-field Hamiltonian will indeed inherit the PSG of the starting one. The second property that we need can be established by considering a decomposition of δH into a piece that commutes with the PSG generators and another piece that does not. It is straightforward to see that terms from quadratic order and beyond must give rise to a potential which is even in powers of the non-PSG conserving piece of δH. Finally, at sufficiently small J_{ij} the potential for the χ_{ij} must be stable due to the explicit factors of $1/J_{ij}$. Together these properties imply that the new minimum must be in the "direction" selected by the linear term and hence will exhibit the same PSG as before.

V. PSG OF THE MONOPOLE FLUX STATE

We will now describe the PSG of the monopole flux state, and its implications for stability at the mean-field level. The space group of the pyrochlore lattice is $Fd\bar{3}m$, which contains 24 symmorphic and 24 nonsymmorphic elements. For our purposes it is most convenient to divide these elements into the 24 proper elements composed of rotations and translations and 24 improper elements involving a reflection or inversion. The 24 proper elements are

$$P^0 = \{1, 8C_3, 3C_2, 6\tilde{C}_2, 6\tilde{C}_4\}. \quad (25)$$

The improper elements consist of

$$P^i = \{i, 8\tilde{S}_6, 3\tilde{\sigma}_h, 6\sigma_d, 6S_4\}, \quad (26)$$

where $\tilde{g}$ denotes a nonsymmorphic operation, in which rotations or reflections are accompanied by translation along an appropriate fraction of a lattice vector. P^0 is a proper subgroup of $Fd\bar{3}m$, while P^i is generated by the product of the inversion operator (inversion is taken about one of the lattice sites) with the elements of P^0. The symmetry transformations, along with the full action of the PSG, are outlined in Appendix B.

The PSG of the monopole flux state has the following general structure, outlined in more detail in Appendix B:

(i) Translations: FCC translations, combined with the identity gauge transformation.

(ii) P^0 space-group elements: These elements are symmetries when combined with appropriate gauge transformations, which induce a π phase shift at some the sites in the unit cell.

(iii) P^i space-group elements: These elements are symmetries when combined with an appropriate gauge transformation, as above, and a time-reversal transformation.

(iv) Charge conjugation C: The charge-conjugation operator maps $c_i \rightarrow c_i^{\dagger}$.

A. Restricting perturbative corrections using PSG invariance

To deduce what restrictions PSG invariance imposes on the spectrum, we begin with a generic 4×4 quadratic Hamiltonian

$$H^{(2)} = \sum_{ij} J_{ij}c_i^{\dagger}c_j. \quad (27)$$

The bonds J_{ij} connect arbitrary sites in the lattice, but respect the lattice symmetries. In what follows, we will use the PSG to restrict the possible quadratic terms, and show that all terms allowed by symmetry vanish at the Fermi surface. Hence the Fermi surface of the monopole flux state is unaffected by PSG-preserving perturbations to the Hamiltonian. For simplicity we will drop the superscript $^{(2)}$ in the remainder of this section to simplify the notation.

Though the inversion P and time reversal T are broken in the mean-field state, the combination PT leaves both the full and mean-field Hamiltonians invariant. Terms invariant under this transformation have the form

$$(J' + iJ'')c_x^\dagger c_{x+\delta} + (J' - iJ'')c_x^\dagger c_{x-\delta}, \tag{28}$$

and the Hamiltonian is real in momentum space. Further, invariance under charge conjugation forces all spatial bonds to be purely imaginary: under C,

$$\begin{aligned}(J' + iJ'')c_x^\dagger c_{x+\delta} + (J' - iJ'')c_{x+\delta}^\dagger c_x \\ \rightarrow (-J' + iJ'')c_x^\dagger c_{x+\delta} + (-J' - iJ'')c_{x+\delta}^\dagger c_x\end{aligned} \tag{29}$$

so that $J'=0$ if C symmetry is unbroken. In momentum space, if we write the Hamiltonian as $\bar{\psi}H(k)\psi$, Eqs. (28) and (29) imply that $H(k)$ is real and an odd function of k. We may express elements of the matrix $H(\mathbf{k})$ as a superposition

$$H_{ab}(\mathbf{k}) = \sum_{\mathbf{R}} J_{\mathbf{R};ab} \sin[\mathbf{k}\cdot(\mathbf{R}+\mathbf{r}_{ab})], \tag{30}$$

where $\mathbf{R}$ is an fcc lattice vector, the indices a,b label sites within the unit cell, and $J_{\mathbf{R};ab}$ is the coupling between sites a and b separated by the lattice vector $\mathbf{R}$ and the vector $\mathbf{r}_{ab}$ in the unit cell. This is the general form for a function periodic in the Brillouin zone.

Diagonal Terms. Let $H_{11}\ldots H_{44}$ be the diagonal elements of H. To restrict the form of H_{11}, we consider the action of all PSG operations that map site 1 in the tetrahedral unit cell onto itself. These are (see Appendix B for labels and actions of the PSG elements) $\{C_1, C_1^2, \tilde{C}_{23}, \tilde{C}_{24}, \tilde{C}_{34}\}$, which transform H_{11} in the following way:

$$\begin{aligned}H_{11}(k_x,k_y,k_z) &\xrightarrow{C_1} H_{11}(k_z,k_x,k_y) \\ &\xrightarrow{C_1^2} H_{11}(k_y,k_z,k_x) \\ &\xrightarrow{\tilde{C}_{23}} H_{11}(-k_x,-k_z,-k_y) \\ &\xrightarrow{\tilde{C}_{24}} H_{11}(-k_z,-k_y,-k_x) \\ &\xrightarrow{\tilde{C}_{34}} H_{11}(-k_y,-k_x,-k_z),\end{aligned} \tag{31}$$

which allows us to express H_{11} in a form where its symmetries are manifest as

$$\begin{aligned}H_{11}(k_x,k_y,k_z) = \frac{1}{6}[&H_{11}(k_x,k_y,k_z) + H_{11}(k_z,k_x,k_y) \\ &+ H_{11}(k_y,k_z,k_x) - H_{11}(k_x,k_z,k_y) - H_{11}(k_z,k_y,k_x) \\ &- H_{11}(k_y,k_x,k_z)].\end{aligned} \tag{32}$$

Similarly we can relate H_{22}, H_{33}, and H_{44} to H_{11} by considering operations which interchange site 1 with sites 2, 3, and 4, respectively. These imply

$$\begin{aligned}H_{22}(k_x,k_y,k_z) &= H_{11}(k_y,k_x,-k_z), \\ H_{33}(k_x,k_y,k_z) &= H_{11}(k_z,-k_y,k_x), \\ H_{44}(k_x,k_y,k_z) &= H_{11}(-k_x,k_z,k_y).\end{aligned} \tag{33}$$

While multiple transformations map between each pair of diagonal elements, the group structure and invariance of H_{11} under PSG transformations ensures that these mappings all yield the same result.

The reader should note that Eqs. (32) and (33) ensure that along the Fermi lines $\mathbf{k}=\pm(1,\pm 1,\pm 1)$ all allowed diagonal terms vanish.

It is worth digressing to make one more comment on the diagonal terms. Using the symmetrized form of H_{11} in Eq. (32) above, we can rewrite the term in Eq. (30) with a fixed $\mathbf{R}$ and $a=b=1$ as

$$\begin{aligned}J_{\mathbf{R};11}\sin(\mathbf{k}\cdot\mathbf{R}) = \frac{1}{6}J_{\mathbf{R};11}[&\sin(k_xR_x + k_yR_y + k_zR_z) \\ &+ \sin(k_zR_x + k_xR_y + k_yR_z) \\ &+ \sin(k_yR_x + k_zR_y + k_xR_z) \\ &- \sin(k_xR_x + k_zR_y + k_yR_z) \\ &- \sin(k_zR_x + k_yR_y + k_xR_z) \\ &- \sin(k_yR_x + k_xR_y + k_zR_z)].\end{aligned} \tag{34}$$

Expressions of the form (34) vanish if any two coefficients are equal; nonvanishing terms occur only for a sum of at least three fcc translations. Physically this corresponds to a hopping between a site and its translate some three lattice vectors distant.

Off-Diagonal Terms. As H is real in momentum space, $H_{ab}=H_{ba}$. To restrict the form of H_{12}, consider the action of all PSG elements which either map sites 1 and 2 to themselves, or interchange them. These are $\{\tilde{C}_{34}, \tilde{C}_{12}, C_z\}$, which transform H_{12} according to

$$\begin{aligned}H_{12}(k_x,k_y,k_z) &\xrightarrow{\tilde{C}_{34}} -H_{12}(-k_y,-k_x,-k_z) \\ &\xrightarrow{\tilde{C}_{12}} H_{21}(k_y,k_x,-k_z) \\ &\xrightarrow{C_z} -H_{21}(-k_x,-k_y,k_z).\end{aligned} \tag{35}$$

Again, transformations mapping sites 1 and 2 onto other sites in the unit cell can be used to deduce the form of the remaining off-diagonal elements. Hence

$$\begin{aligned}H_{12}(k_x,k_y,k_z) &\xrightarrow{C_1} H_{13}(k_z,k_x,k_y) \\ &\xrightarrow{C_1^2} H_{14}(k_y,k_z,k_x) \\ &\xrightarrow{C_4^2} -H_{23}(-k_y,k_z,-k_x) \\ &\xrightarrow{C_2} -H_{24}(-k_z,k_x,-k_y) \\ &\xrightarrow{C_y} -H_{34}(-k_x,k_y,-k_z)\end{aligned} \tag{36}$$

This gives off-diagonal entries

$$\begin{bmatrix} 0 & H_{12}(k_x,k_y,k_z) & H_{12}(k_z,k_x,k_y) & H_{12}(k_y,k_z,k_x) \\ H_{12}(k_x,k_y,k_z) & 0 & H_{12}(k_y,-k_z,k_x) & H_{12}(k_z,-k_x,k_y) \\ H_{12}(k_z,k_x,k_y) & H_{12}(k_y,-k_z,k_x) & 0 & H_{12}(k_x,-k_y,k_z) \\ H_{12}(k_y,k_z,k_x) & H_{12}(k_z,-k_x,k_y) & H_{12}(k_x,-k_y,k_z) & 0 \end{bmatrix}, \tag{37}$$

where again we can make the symmetries manifest by writing

$$H_{12}(k_x,k_y,k_z) = \frac{1}{4}[H_{12}(k_x,k_y,k_z) + H_{12}(k_y,k_x,k_z) + H_{12}(k_y,k_x,-k_z) + H_{12}(k_x,k_y,-k_z)]. \tag{38}$$

Again, it is useful to focus on the contribution to H_{12} from bonds with a given $\mathbf{R}$, which can now be seen to come with the factor

$$\cos(k_z R_z)\left[\sin\left(k_x R_x + k_y R_y + \frac{k_x+k_y}{2}\right) + \sin\left(k_y R_x + k_x R_y + \frac{k_x+k_y}{2}\right)\right]. \tag{39}$$

Equation (39) shows that $H_{12}(k_x,k_y,k_z)$ vanishes along the lines $(k,-k,-k),(-k,k,-k)$. Of course, this can also be seen directly from Eq. (38).

Now we may consider the fate of the monopole flux state's exotic Fermi surface. Since PSG rotations map between different Fermi lines, it is sufficient to consider possible alterations to the spectrum on Fermi line (k,k,k). The most general form that H can have about the line (k,k,k) is

$$H = \begin{bmatrix} 0 & H_{12}(k,k,k) & H_{12}(k,k,k) & H_{12}(k,k,k) \\ H_{12}(k,k,k) & 0 & 0 & 0 \\ H_{12}(k,k,k) & 0 & 0 & 0 \\ H_{12}(k,k,k) & 0 & 0 & 0 \end{bmatrix}, \tag{40}$$

which has two zero eigenvalues. Thus terms allowed by symmetry add neither a chemical potential nor a gap to any part of the Fermi lines, and preserve the characteristic structure of the monopole flux state, with two low-energy states about each Fermi line and four low-energy states about the origin.

Note that nothing prevents the Fermi velocity v_F from being modified as a function of the momentum along the line. Indeed, Eq. (40) implies that the general form of v_F is

$$\frac{v_F(k)}{\sqrt{2}} = \sum_{\mathbf{R}} J_{\mathbf{R};12}(R_x + R_y + 1/2)\cos(2kR_z)\cos 2k(R_y - R_x) + \frac{J_{\mathbf{R};11}}{3}[R_x \sin(2kR_x)\sin 2k(R_z - R_y) + R_y \sin(2kR_y)\sin 2k(R_x - R_z) + R_z \sin(2kR_z)\sin 2k(R_y - R_x)]. \tag{41}$$

B. Time reversal and parity

One striking feature of H_{MF} is that it is *odd* under both T and P, reminiscent of the chiral spin state first described in Ref. 21. Though T is naively broken, some care must be taken to show that the apparent T breaking is physical and that $|\psi\rangle, T|\psi\rangle$ are gauge inequivalent states.[36] Readers familiar with this subtlety from discussions of T breaking on the square lattice should note that the pyrochlore lattice is not bipartite, and hence naive time reversal is no longer equivalent to particle-hole conjugation. But most directly, as explained in Ref. 21, the operator

$$E_{ijk} = S_i \cdot (S_j \times S_k), \tag{42}$$

where the spins i, j, and k lie in a triangular plaquette, is odd under T and P. Hence if $\langle E_{ijk}\rangle_{|\psi\rangle} \neq 0$, the state $|\psi\rangle$ breaks time reversal.

At mean-field level,

$$\frac{-i}{2}\langle E_{123}\rangle = \langle \chi_{12}\chi_{23}\chi_{31}\rangle - \langle \chi_{13}\chi_{32}\chi_{21}\rangle \tag{43}$$

and states with an imaginary flux through triangular plaquettes are T breaking. For the monopole flux state, we have confirmed numerically that this T breaking in each plaquette is robust to Gutzwiller projection; the results are shown in Table II.

We also note the curiosity that at infinite N, the spectrum-preserving nature of T and P allows us to construct additional symmetries which are *not*, however, symmetries of the full H. Particle-hole symmetry at each k allows us to construct the following two discrete symmetries of H_{MF}:

$$\tilde{T}: |\psi(x,t)\rangle \to \alpha^{(0)}|\psi(x,-t)\rangle,$$

$$\tilde{P}: |\psi(x,t)\rangle \to \alpha^{(0)}|\psi(-x,t)\rangle, \tag{44}$$

where α^0 was defined in Eq. (17). Both of these commute with the noninteracting Hamiltonian: since $\alpha_0^{-1} H \alpha_0 = -H$, we have

TABLE II. Expectation values of the T-breaking operator $\langle E_\Delta\rangle$ for triangular faces of the tetrahedra.

Lattice size	$\langle E_\Delta\rangle$
$3\times3\times3$	0.039
$5\times5\times5$	0.043

$$\langle\psi|\tilde{T}^{\dagger}H\tilde{T}|\psi\rangle = -\langle\psi|H^{*}|\psi\rangle = \langle\psi|H|\psi\rangle,$$

$$\langle\psi|\tilde{P}^{\dagger}H\tilde{P}|\psi\rangle = -\langle\psi|H^{T}|\psi\rangle = \langle\psi|H|\psi\rangle. \quad (45)$$

The matrix structure of α_0 is such that $\tilde{T}$ and $\tilde{P}$ are not symmetries of the full Hamiltonian, however, and will not be robust to perturbative corrections about mean field.

C. PSG symmetry and perturbation theory in the long-wavelength limit

We have established that invariance under the PSG transformations and charge conjugation forbid both mass and chemical-potential terms on the Fermi lines. Here we explore how these PSG symmetries are realized as symmetries of the linearized low-energy theory away from the origin, and hence see in that setting why they are protected perturbatively.

Consider the linearized theory about the Fermi line $\boldsymbol{l_1}=(k,k,k)$. A general Hamiltonian in the 2×2 space of low-energy states can be expressed as

$$H(\mathbf{k}) = \psi_1^{\dagger}(\mathbf{k})h(\mathbf{k})\psi_1(\mathbf{k}),$$

$$h(\mathbf{k}) = \mu(k) + m(k)\sigma_3 + \varepsilon(k,v)[\cos(\theta)\sigma_1 + \sin(\theta)\sigma_2], \quad (46)$$

where k is the component of the momentum $\mathbf{k}$ along the line and (v,θ) are the magnitude and angle, respectively, of the momentum perpendicular to the line. Here

$$\psi_{11}(\mathbf{k}) = (0,\omega^2,1,\omega)\cdot\boldsymbol{c_\alpha}(\mathbf{k}),$$

$$\psi_{12}(\mathbf{k}) = (0,\omega,1,\omega^2)\cdot\boldsymbol{c_\alpha}(\mathbf{k}), \quad (47)$$

with $\omega=e^{2\pi i/3}$. The states (47) are eigenstates of the rotation operator C_1 which rotates about the (1,1,1) direction, with $C_1\psi_{1j}=\omega^j\psi_{1j}$.

Under charge conjugation,

$$\psi_{11}(\mathbf{k}) \to \psi_{12}^{\dagger}(-\mathbf{k}),$$

$$\psi_{12}(\mathbf{k}) \to \psi_{11}^{\dagger}(-\mathbf{k}). \quad (48)$$

The corresponding symmetry operator in the continuum theory is

$$C{:}\psi_1(v,\theta) \to \sigma_1[\psi_1^{\dagger}(v,\pi-\theta)]^T \quad (49)$$

with the Fermi surface points at k and $-k$ interchanged. This implies $m(-k)=m(k)$ and $\mu(-k)=-\mu(k)$.

Further, an analysis of the PSG transformations reveals that the glide rotations $(\tilde{C}_{ij})$ map clockwise rotating states to counterclockwise states while reversing the direction of the corresponding Fermi line: $\psi_{i1}(kl_i)\to\psi_{i2}(-kl_i)$. This transformation leaves the mean-field Hamiltonian invariant. In the 2×2 basis, this is because

$$T{:}|\psi(v,\theta)\rangle \to \sigma_1|\psi(v,\pi-\theta)\rangle \quad (50)$$

is a symmetry of the mean-field Hamiltonian. Note that the momentum transformation can be realized in three dimensions by a π rotation about the line $x=y$, and hence should also send $k\to -k$, though there is no way to deduce this from the form of the mean-field eigenstates. The symmetry transformation (50) reverses the sign of the mass term, but not of the chemical potential, implying that $m(-k)=-m(k)$ and $\mu(k)=\mu(-k)$. Hence we conclude that in the continuum theory about a given Fermi line, the symmetries C and T prevent a gap or chemical potential from arising.

One might ask why we have not considered mass gaps of the form $m\sigma_1$ or $m\sigma_2$; both of these choices turn out to violate either Eq. (49) or (50). Indeed, both choices explicitly break the rotational symmetry of the spectrum about the Fermi line.

VI. CONCLUDING REMARKS

We have discussed an interesting mean-field (large-N) solution to the Heisenberg model on the pyrochlore lattice. This is a P- and T-breaking state in which all triangular plaquettes have an outward flux of $\pi/2$. After Gutzwiller projection, this state has lower energy than all other mean-field states considered, including the simplest dimerized state. Its low-energy physics is rather striking, with a spinon Fermi surface of lines of nodes preserving the discrete rotational symmetries of the lattice. The symmetries of the Hamiltonian suggest that this Fermi surface is perturbatively stable and thus should characterize a stable spin-liquid phase, at least at sufficiently large N.

However, our analysis of stability is thus far based only on symmetries and does not rule out dynamical instabilities. The study of such instabilities requires adding back in the gauge fluctuations that are suppressed at $N=\infty$ and studying the coupled system consisting of spinons and gauge fields. In the well-studied case of two-dimensional algebraic spin liquids it took a while to understand that this coupled system could, in fact, support a gapless phase at sufficiently large N despite the compactness of the gauge fields. In the present problem there is also the specific feature that at $N=2$, as the background flux per plaquette is U(1), such an analysis should incorporate fluctuations of an SU(2) gauge field.[24] We defer addressing this set of questions to future work.[25] We do note though that the applicability of our ideas to the strict case of $N=2$ will ultimately have to be tested either in actual experiments looking for T and P breaking and for the distinctive spinon spectrum of nodal lines, or in numerical work looking for the same features, e.g., computations of the correlations of the triple product operator in Eq. (42). Spinon Fermi lines could be detected directly through neutron scattering, or indirectly through measurements of the specific heat, which for noninteracting Fermi lines in three dimensions is quadratic in T.

Finally, we note that our initial motivation in this study was to see if we could construct a fully symmetric spin liquid on the pyrochlore lattice for $S=1/2$ in contradiction with previous studies using other techniques. We have not succeeded in that goal and, as the technique in this paper has produced a pattern of symmetry breaking distinct from the ones considered previously, the fate of the $S=1/2$ nearest-neighbor Heisenberg antiferromagnet on the pyrochlore lattice remains indecipherable.

ACKNOWLEDGMENTS

We are grateful to R. Shankar for his collaboration on closely related work. We would like to thank Eduardo Fradkin, Roderich Moessner, Ashvin Vishwanath, and Michael Hermele for instructive discussions. We would also like to acknowledge support from NSF under Grant No. DMR 0213706. F.J.B. acknowledges the support of NSERC.

APPENDIX A: MONTE CARLO AND PROJECTED WAVE FUNCTIONS

Gutzwiller projection can be carried out exactly for finite systems using the projector in the Slater determinant basis, using the method of Ref. 32. At half filling, the Slater determinant is represented as a product of a spin-up and a spin-down determinant of equal size $(N/2)$, where N is the number of sites in the lattice. Each site is represented exactly once in either the spin-up or the spin-down matrix, yielding a wave function which obeys the single occupation constraint on all lattice sites and is a total spin singlet. The problem then reduces to the evaluation of expectation values of operators for wave functions of finite systems with definite spin distributions on the lattice

$$\langle O\rangle = \frac{\langle\psi|O|\psi\rangle}{\langle\psi|\psi\rangle}, \tag{A1}$$

where $|\psi\rangle = \Sigma_\alpha \langle\alpha|\psi\rangle|\alpha\rangle$ and $|\alpha\rangle$ is a specific distribution of spins on the lattice

$$|\alpha\rangle = \prod_i c^\dagger_{R_i,\uparrow} \prod_j c^\dagger_{R_j,\downarrow}|0\rangle. \tag{A2}$$

The expectation value of the operator O is evaluated by summing over all spin configurations on the lattice. To evaluate this sum we follow the approach of Ref. 32, which we will review here. The expectation value is given by

$$\langle O\rangle = \sum_\alpha \left(\sum_\beta \frac{\langle\alpha|O|\beta\rangle\langle\beta|\psi\rangle}{\langle\alpha|\psi\rangle}\right)\frac{|\langle\alpha|\psi\rangle|^2}{\langle\psi|\psi\rangle} = \sum_\alpha f(\alpha)\rho(\alpha), \tag{A3}$$

where

$$f(\alpha) = \sum_\alpha \left(\sum_\beta \frac{\langle\alpha|O|\beta\rangle\langle\beta|\psi\rangle}{\langle\alpha|\psi\rangle}\right), \tag{A4a}$$

$$\rho(\alpha) = \frac{|\langle\alpha|\psi\rangle|^2}{\langle\psi|\psi\rangle}. \tag{A4b}$$

Here $\rho(\alpha)\geq 0$ and $\Sigma_\alpha\rho(\alpha)=1$, which makes $\rho(\alpha)$ a probability distribution. The expectation value can be rewritten to resemble a weighted sample, with weights given by $\rho(\alpha)$ and evaluated using a Monte Carlo sampling. The evaluation is executed using a random walk in configuration space with the weight $\rho(\alpha)$. The transition probability $T_{\alpha\alpha'}$ of the Monte Carlo step is

$$T_{\alpha\alpha'} = \begin{cases} 1 & \rho(\alpha') > \rho(\alpha) \\ \rho(\alpha')/\rho(\alpha) & \rho(\alpha') < \rho(\alpha). \end{cases} \tag{A5}$$

The configuration α' is generated by exchanging a randomly selected pair of oppositely oriented spins. We also calculate various operators in the mean-field wave function to test the accuracy of the algorithm. In this case the one particle per site constraint is not imposed; the configuration α' is generated by moving an up or down electron at random to another empty up or down site.

Pyrochlore has an fcc lattice with a four-point basis. We use the rhombohedral unit cell for the Monte Carlo evaluation, using boundary conditions periodic along the fcc directions. The spin correlations turn out to be quite insensitive to boundary conditions for the lattice sizes that we have considered.

To compute the Slater determinant, the mean-field Hamiltonian (10) is diagonalized in the band eigenstates

$$H = \sum_{a,b,\boldsymbol{k}} c^{\dagger\alpha}_{a\boldsymbol{k}} H_{ab}(\boldsymbol{k}) c_{b\boldsymbol{k}\alpha} = \sum_{\nu\boldsymbol{k}} E_\nu(\boldsymbol{k}) a^{\dagger\alpha}_{\nu\boldsymbol{k}} a_{\nu\boldsymbol{k}\alpha}, \tag{A6}$$

where $c^{\dagger\alpha}_{a\boldsymbol{k}}$ is the Fourier transform

$$c^{\dagger\alpha}_{a\boldsymbol{k}} = \sum_{\boldsymbol{k}} e^{i\boldsymbol{k}\cdot(\boldsymbol{R}_i + \boldsymbol{r}_{a_i}/2)} c^{\dagger\alpha}_{\boldsymbol{R}_i + \boldsymbol{r}_{a_i}/2}. \tag{A7}$$

Here $\boldsymbol{r}_{a_i}/2$ refer to the points in the four site basis of the tetrahedral unit cell. If we assume that the bands $\nu=1,2$ are filled, the operator $c^{\dagger\alpha}_{a\boldsymbol{k}}$ can be expressed as

$$c^{\dagger\alpha}_{a\boldsymbol{k}} = S_{a,1}(\boldsymbol{k}) a^{\dagger\alpha}_{1,\boldsymbol{k}} + S_{a,2}(\boldsymbol{k}) a^{\dagger\alpha}_{2,\boldsymbol{k}}, \tag{A8}$$

where the matrix $S^\dagger_{a,\nu}(\boldsymbol{k})$ diagonalizes the Hamiltonian. The mean-field ground state is just the Fermi sea filled to the appropriate Fermi level which, in this case, is the first Brillouin-zone boundary,

$$|\Phi\rangle_{\text{mean}} = \prod_{\boldsymbol{k}<\boldsymbol{k}_f,\alpha} a^{\dagger\alpha}_{1,\boldsymbol{k}} a^{\dagger\alpha}_{2,\boldsymbol{k}}|0\rangle. \tag{A9}$$

We rewrite the mean-field Fermi sea $|\Phi\rangle_{\text{mean}}$ in first quantized form,

$$\Phi = \sum_{U,D} \Phi_{U\uparrow}\Phi_{D\downarrow}|U\rangle|D\rangle, \tag{A10}$$

where

$$|U\rangle = c^\dagger_{\boldsymbol{R}_{1,a_1}\uparrow} \cdots c^\dagger_{\boldsymbol{R}_{N_L/2,a_{N_L/2}}\uparrow}|0\rangle, \tag{A11}$$

$$|D\rangle = c^\dagger_{\boldsymbol{R}'_{1,a_1}\downarrow} \cdots c^\dagger_{\boldsymbol{R}'_{N_L/2,a_{N_L/2}}\downarrow}|0\rangle. \tag{A12}$$

The basic Slater determinant wave function for each spin orientation is of the form

$$\Phi(\boldsymbol{R}_{i,a_i}:\boldsymbol{k}_j,\nu)_\alpha = \text{Det}[\phi(\boldsymbol{R}_{i,a_i}:\boldsymbol{k}_j,\nu)]_\alpha, \tag{A13}$$

where $\phi(\boldsymbol{R}_{i,a_i}:\boldsymbol{k}_j,\nu)$ is the single-particle wave function of the electron at $\boldsymbol{R}_{i,a_i}=\boldsymbol{R}_i+\boldsymbol{r}_{a_i}/2$. The wave number $\boldsymbol{k}_j$ refers to a point in the conjugate lattice in the rhombohedral Brillouin zone and ν is the band index. In terms of the matrix $S_{a,\nu}(\boldsymbol{k})$, the single-particle wave function is

TABLE III. Spin Correlations from variational Monte Carlo. To check the accuracy of the algorithm, correlators are also calculated at mean-field, using both Monte Carlo (MC) and Green's function (G) approaches.

Trial wave function	$S_1^z S_2^z$	$S_1^z S_3^z$	$S_1^z S_4^z$	$S_1^z S_5^z$
Mean field				
Flux (G)	−0.01388	−0.00188	−0.00097	−0.00097
Flux (MC)	−0.01386	−0.00192	−0.00103	−0.00084
	±0.00003	±0.00004	±0.00005	±0.00006
Monopole (G)	−0.01745	0.00000	0.00000	−0.00087
Monopole (MC)	−0.01713	−0.00002	−0.00008	−0.00085
	±0.00004	±0.00001	±0.00002	±0.00006
Projected				
Flux	−0.04169	−0.00137	0.0029	−0.00270
	±0.00004	±0.00005	±0.0001	±0.00008
Monopole	−0.0497	0.00631	0.00528	−0.00499
	±0.0001	±0.00002	±0.00004	±0.00005

$$\phi(\boldsymbol{R}_{i,a_i}:\boldsymbol{k}_j,\nu) = S_{a,\nu}(\boldsymbol{k}_j)e^{i\boldsymbol{k}_j\cdot(\boldsymbol{R}_i+\boldsymbol{r}_{a_i}/2)}. \tag{A14}$$

In the above, $U=\{\boldsymbol{R}_{\mathbf{1},a_\mathbf{1}},\ldots,\boldsymbol{R}_{N_L/2,a_{N_L/2}}\}$ is the set of lattice sites occupied by up-spin electrons, and $D=\{\boldsymbol{R}'_{\mathbf{1},a_\mathbf{1}},\ldots,\boldsymbol{R}'_{N_L/2,a_{N_L/2}}\}$ is the set of lattice sites occupied by down-spin electrons.

Gutzwiller projection is imposed by ensuring that the two sets U and D have no elements in common. The Monte Carlo update is performed by exchanging rows selected at random from the $\Phi_{U\uparrow}$ and $\Phi_{D\downarrow}$ matrices.

The calculation of the transition probability $T_{\alpha\alpha'}$ involves the calculation of determinants of matrices of size $N_L/2\times N_L/2$, an $O(N_L^3)$ operation. The algorithm of Ceperley *et al.*[37] reduces this to an $O(N_L^2)$ operation for the special case of updates involving one row or column. The matrix $M^U=\Phi_{U\uparrow}$ and the transpose of its inverse $\bar{M}^U$ (similarly for $\Phi_{D\downarrow}$) are stored at the beginning of the Monte Carlo evolution. If the update changes the ath row $M^U_{aj}\to A_j$, $M^U\to M'^U$, the transition matrix is $T_{\alpha\alpha'}=\mathrm{Det}\,M'^U/\mathrm{Det}\,M^U$,

$$\frac{\mathrm{Det}\,M'^U}{\mathrm{Det}\,M^U} = \sum_{j=1}^{N_L/2} A_j \bar{M}^U_{ja} = r. \tag{A15}$$

This is due to the fact that $\mathrm{Det}(M^U\bar{M}^U)$ is the matrix of cofactors. If the move is accepted, the inverse matrix can be updated using $O(N_L^2)$ operations,

$$\bar{M}^U_{ji} = \begin{cases} \bar{M}^U_{ji}/r & i=a \\ \bar{M}^U_{ji} - \bar{M}^U_{ja}\sum_{k=1}^{N_L/2} A_k \bar{M}^U_{kj}/r & i\neq a. \end{cases} \tag{A16}$$

The evaluation of operator expectations values has to be handled with care as we are dealing with fermions. The relative sign of determinants must be tracked in a consistent way. Thus we write all spin configurations in the order

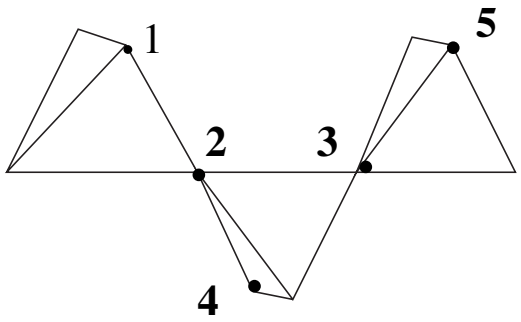

FIG. 4. Sites for the spin-correlation functions calculated in Table III.

$$|\alpha\rangle = c^\dagger_{\boldsymbol{R}_{\mathbf{1},a_\mathbf{1}}\uparrow}\cdots c^\dagger_{\boldsymbol{R}_{N_L/2,a_{N_L/2}}\uparrow},\quad c^\dagger_{\boldsymbol{R}'_{\mathbf{1},a_\mathbf{1}}\downarrow}\cdots c^\dagger_{\boldsymbol{R}'_{N_L/2,a_{N_L/2}}\downarrow}|0\rangle. \tag{A17}$$

The wave function is given by $\langle\Phi|\alpha\rangle=\Phi_{U\uparrow}\Phi_{D\downarrow}(\alpha)$, the Slater determinant eigenfunction with the given spin distribution α. We are interested in the operators $\Sigma S^z_{\boldsymbol{R}_{i,a_i}}\cdot S^z_{\boldsymbol{R}_{j,a_j}}$ and $\Sigma(S^+_{\boldsymbol{R}_{i,a_i}}\cdot S^-_{\boldsymbol{R}_{j,a_j}}+S^-_{\boldsymbol{R}_{i,a_i}}\cdot S^+_{\boldsymbol{R}_{j,a_j}})$. To keep track of the proper sign specification we express the spin operators in terms of fermionic operators with the same order as the spin configuration,

$$S^z_{\boldsymbol{R}_{i,a_i}}\cdot S^z_{\boldsymbol{R}_{j,a_j}} = (n_{\boldsymbol{R}_{i,a_i}\uparrow}-n_{\boldsymbol{R}_{i,a_i}\downarrow})(n_{\boldsymbol{R}_{j,a_j}\uparrow}-n_{\boldsymbol{R}_{j,a_j}\downarrow})/4, \tag{A18}$$

$$S^+_{\boldsymbol{R}_{i,a_i}}\cdot S^-_{\boldsymbol{R}_{j,a_j}} = c^\dagger_{\boldsymbol{R}_{i,a_i}\uparrow}c_{\boldsymbol{R}_{i,a_i}\downarrow}c^\dagger_{\boldsymbol{R}_{j,a_j}\uparrow}c_{\boldsymbol{R}_{j,a_j}\downarrow}, \tag{A19}$$

$$= -c^\dagger_{\boldsymbol{R}_{i,a_i}\uparrow}c^\dagger_{\boldsymbol{R}_{j,a_j}\uparrow}c_{\boldsymbol{R}_{i,a_i}\downarrow}c_{\boldsymbol{R}_{j,a_j}\downarrow}. \tag{A20}$$

The amplitude $S^+_{\boldsymbol{R}_{i,a_i}}\cdot S^-_{\boldsymbol{R}_{j,a_j}}|\alpha\rangle$ is the determinant wave function $\Phi_{U\uparrow}\Phi_{D\downarrow}(\alpha')$ with the rows of $\Phi_{U\uparrow}$ and $\Phi_{D\downarrow}$ changed as described above. $S^z_{\boldsymbol{R}_{i,a_i}}\cdot S^z_{\boldsymbol{R}_{j,a_j}}|\alpha\rangle$ is easier to evaluate as it is diagonal.

As a result of the four-site basis there are only $N_L/4$ lattice points in the Brillouin zone. Therefore, the accuracy of the Monte Carlo evaluation is limited by the number of points in $\boldsymbol{k}$ space. We have used a lattices of size $5\times5\times5$ (500 sites).

A basic Monte Carlo "move" consists of $2N_L$ updates followed by a sampling. The first 10 000 moves were used for thermal relaxation and were discarded. 50 000 samples were used for the evaluation of expectation values. These were divided into ten sets and the average in each set was used to estimate the statistical fluctuations and error bars of the Monte Carlo evaluation. To check the accuracy of the algorithm and the effect of finite lattice size we evaluated spin-correlation functions of the mean-field states and compared with results from the numerical evaluation of Green's functions. The Monte Carlo results are quite close to the expected values (see Table III). The site indices of the spins refers to Fig. 4.

TABLE IV. Action of PSG point-group rotations on spinon operators.

1	C_1	C_1^2	C_2	C_2^2	C_3	C_3^2	C_4	C_4^2	C_x	C_y	C_z
c_1	c_1	c_1	c_4	$-c_3$	c_2	$-c_4$	c_3	$-c_2$	$-c_4$	$-c_3$	c_2
c_2	c_3	c_4	$-c_2$	$-c_2$	c_4	c_1	$-c_1$	c_3	$-c_3$	c_4	$-c_1$
c_3	c_4	c_2	$-c_1$	c_4	$-c_3$	$-c_3$	c_2	c_1	c_2	c_1	c_4
c_4	c_2	c_3	c_3	c_1	$-c_1$	c_2	$-c_4$	$-c_4$	c_1	$-c_2$	$-c_3$
k_x	k_z	k_y	$-k_z$	k_y	k_z	$-k_y$	$-k_z$	$-k_y$	k_x	$-k_x$	$-k_x$
k_y	k_x	k_z	k_x	$-k_z$	$-k_x$	$-k_z$	$-k_x$	k_z	$-k_y$	k_y	$-k_y$
k_z	k_y	k_x	$-k_y$	$-k_x$	$-k_y$	k_x	k_y	$-k_x$	$-k_z$	$-k_z$	k_z

APPENDIX B: THE PSG OF THE MONOPOLE FLUX STATE

1. Symmetries of the pyrochlore lattice

The space group $Fd\bar{3}m$ of the pyrochlore lattice consists of the 24-element tetrahedral point group $\bar{4}3m$, and a further 24 nonsymmorphic elements. We will briefly describe the actions of these symmetry operations here. All vectors are expressed in the basis of the standard cubic fcc unit cell.

The actions of the tetrahedral point group fix the position of one tetrahedron's center [at, e.g., $(a/8,a/8,a/8)$]. Its elements are:

(1) The identity;

(2) $8C_3$: there are four threefold axes, one passing through each vertex and the center of the opposite face. Rotations about this axis permute the three vertices not on the axis. These we label $C_1 \ldots C_4$ and $C_1^2 \ldots C_4^2$, where C_i, C_i^2 fix site i of the tetrahedral unit cell.

(3) $3C_2$: There are three twofold axes, parallel to the x, y, and z axes. Each axis bisects a pair of edges on the tetrahedron; the ensuing rotation exchanges pairs of vertices. These we label C_x, C_y, C_z.

(4) $6\sigma_d$: A plane of reflection passes through each edge and out the center of the opposite face. These planes lie on the diagonals with respect to the fcc cubic unit cell, and hence are called diagonal reflections.

(5) $6S_4$: An improper rotation of degree 4 about the axis bisecting two edges (parallel to the x, y, or z axis) is also a symmetry. The tetrahedron is rotated by $\pi/2$ about, e.g., $(1/8,1/8,z)$ and reflected through the plane $z=1/8$. This operation squared produces one of the twofold rotations so each axis contributes two group elements.

The remaining nonsymmorphic elements, which we distinguish from their symmorphic counterparts using the notation $\tilde{S}$, are:

(1) $6\tilde{C}_4$: There are three fourfold screw axes: $(3/8,1/8,z)$, $(3/8,y,1/8)$, and $(x,3/8,1/8)$. The symmetry rotates the lattice by $\pi/4$ about such an axis, and translates by 1/4 of the side length of the fcc cubic unit cell along the axis. Each axis accounts for two elements of the quotient group, as $C_4^2 = tC_2$, with t an fcc translation and C_2 one of the twofold rotations of the point group. These we label $\tilde{C}_x, \tilde{C}_x^2, \tilde{C}_y, \tilde{C}_y^2, \tilde{C}_z, \tilde{C}_z^2$.

(2) $6\tilde{C}_2$: Along each of the six edges of the tetrahedron (the fcc basis vectors) there is a twofold screw axis. The lattice is translated along the edge of a tetrahedron, then rotated by π about this edge. These we label $\tilde{C}_{ij}$, where $\tilde{C}_{ij}$ has a screw axis along the line joining sites i and j.

(3) $3\tilde{\sigma}_h$: The x, y, and z planes of the cubic unit cell each contain a horizontal glide plane. The lattice is translated along an fcc vector in the plane, e.g., by (1/4, 1/4, 0), and then reflected through the plane—in our example, through $z=0$.

(4) i The lattice is inverted about the origin.

(5) $8\tilde{S}_6$: The products of the 8 C_3 rotations with the inversion give eight improper threefold rotations. (These are not in the point group because they map a single tetrahedron onto its neighbor.)

For our purposes these 48 elements divide into 24 C elements involving pure rotations and translations, and 24 S elements involving improper rotations, reflections, or inversions. The S elements are not symmetries of the monopole flux state, as they map monopoles to antimonopoles; to con-

TABLE V. PSG action of screw rotations.

	$\tilde{C}_{12}$	$\tilde{C}_{13}$	$\tilde{C}_{14}$	$\tilde{C}_{23}$	$\tilde{C}_{24}$	$\tilde{C}_{34}$	$\tilde{C}_x$	$\tilde{C}_y$	$\tilde{C}_z$	$\tilde{C}_x^3$	$\tilde{C}_y^3$	$\tilde{C}_z^3$
c_1	c_2	c_3	c_4	$-c_1$	$-c_1$	$-c_1$	c_2	c_4	c_3	c_3	c_2	c_4
c_2	c_1	$-c_2$	c_2	c_3	c_4	c_2	$-c_4$	c_1	c_4	c_1	c_3	$-c_3$
c_3	c_3	c_1	$-c_3$	c_2	c_3	c_4	c_1	c_2	$-c_2$	c_4	$-c_4$	c_1
c_4	$-c_4$	c_4	c_1	c_4	c_2	c_3	c_3	$-c_3$	c_1	$-c_2$	c_1	c_2
k_x	k_y	k_z	$-k_x$	$-k_x$	$-k_z$	$-k_y$	k_x	k_x	k_z	$-k_z$	$-k_y$	k_y
k_y	k_x	$-k_y$	k_z	$-k_z$	$-k_y$	$-k_x$	$-k_z$	k_z	k_y	k_y	k_x	$-k_x$
k_z	$-k_z$	k_x	k_y	$-k_y$	$-k_x$	$-k_z$	k_y	$-k_y$	$-k_x$	k_x	k_z	k_z

TABLE VI. Effect of point-group rotations on low-energy eigenstates.

	C_1	C_2	C_3	C_4	C_x	C_y	C_z
ψ_{11}	$\omega\psi_{11}$	$\omega^2\psi_{31}$	$-\omega\psi_{41}$	$-\omega^2\psi_{21}$	$-\psi_{41}$	$\omega\psi_{31}$	$\omega\psi_{21}$
ψ_{12}	$\omega^2\psi_{12}$	$\omega\psi_{32}$	$-\omega^2\psi_{42}$	$-\omega\psi_{22}$	$-\psi_{42}$	$\omega^2\psi_{32}$	$\omega^2\psi_{22}$
ψ_{21}	ψ_{41}	$\omega\psi_{21}$	ψ_{11}	$\omega\psi_{31}$	$-\psi_{31}$	$-\omega^2\psi_{41}$	$-\omega^2\psi_{11}$
ψ_{22}	ψ_{42}	$\omega^2\psi_{22}$	ψ_{12}	$\omega^2\psi_{32}$	$-\psi_{32}$	$-\omega\psi_{41}$	$-\omega\psi_{12}$
ψ_{31}	$-\omega\psi_{21}$	ψ_{41}	$\omega\psi_{31}$	$-\psi_{11}$	ψ_{21}	$-\omega^2\psi_{11}$	$\omega^2\psi_{41}$
ψ_{32}	$-\omega^2\psi_{22}$	ψ_{42}	$\omega^2\psi_{32}$	$-\psi_{12}$	ψ_{22}	$-\omega\psi_{12}$	$\omega\psi_{42}$
ψ_{41}	$-\omega^2\psi_{31}$	$\omega\psi_{11}$	$-\omega^2\psi_{21}$	$\omega\psi_{41}$	ψ_{11}	$\omega\psi_{21}$	$-\omega\psi_{31}$
ψ_{42}	$-\omega\psi_{32}$	$\omega^2\psi_{12}$	$-\omega\psi_{22}$	$\omega^2\psi_{42}$	ψ_{12}	$\omega^2\psi_{22}$	$-\omega^2\psi_{32}$

struct the appropriate symmetry elements they must be combined with a time-reversal transformation. Since all such elements can be expressed as a product of a C element with the inversion, this is simply a consequence of the fact that while P and T are separately broken in the monopole flux state, the combination PT is still a symmetry.

2. PSG

Here we list in Tables IV and V the PSG transformation rules for the symmetry operations described above. Throughout, we use the gauge illustrated in Fig. 1, in which all bonds are either ingoing or outgoing from site 1; starting from a different gauge will permute the gauge transformations listed here (note that this has no effect on which bonds are allowed or disallowed by the PSG, however). Note that these tables only show the mapping between the site labels 1–4; it is important to bear in mind the effect of the translations in the case of the nonsymmorphic elements, which reverse the directions between sites by interchanging up and down triangles. To this end we also include a table of momentum transformations under these operations.

Since S elements are products of C elements and inversion, it is sufficient to consider the 24 rotation operations, together with the operator iT. Note that group multiplication in the PSG is valid modulo the global gauge transformation $c_i \rightarrow -c_i$, which clearly does not alter the Hamiltonian. Thus only the relative phases of the four sites in the tetrahedral unit cell are relevant to the PSG transformation.

TABLE VII. Effect of twofold glide rotations on low-energy eigenstates.

	$\tilde{C}_{12}$	$\tilde{C}_{13}$	$\tilde{C}_{14}$	$\tilde{C}_{23}$	$\tilde{C}_{24}$	$\tilde{C}_{34}$
ψ_{11}	$\omega\psi_{22}$	$\omega^2\psi_{32}$	$-\omega\psi_{42}$	$-\omega^2\psi_{12}$	$-\psi_{12}$	$\omega\psi_{12}$
ψ_{12}	$\omega^2\psi_{21}$	$\omega\psi_{31}$	$-\omega^2\psi_{41}$	$-\omega\psi_{11}$	$-\psi_{11}$	$\omega^2\psi_{11}$
ψ_{21}	ψ_{12}	$\omega\psi_{22}$	ψ_{22}	$\omega\psi_{32}$	$-\psi_{42}$	$-\omega^2\psi_{22}$
ψ_{22}	ψ_{11}	$\omega^2\psi_{21}$	ψ_{21}	$\omega^2\psi_{31}$	$-\psi_{41}$	$-\omega\psi_{22}$
ψ_{31}	$-\omega\psi_{32}$	ψ_{12}	$\omega\psi_{32}$	$-\psi_{22}$	ψ_{32}	$-\omega^2\psi_{42}$
ψ_{32}	$-\omega^2\psi_{31}$	ψ_{11}	$\omega^2\psi_{31}$	$-\psi_{21}$	ψ_{31}	$-\omega\psi_{41}$
ψ_{41}	$-\omega^2\psi_{42}$	$\omega\psi_{42}$	$-\omega^2\psi_{12}$	$\omega\psi_{42}$	ψ_{22}	$\omega\psi_{32}$
ψ_{42}	$-\omega\psi_{41}$	$\omega^2\psi_{41}$	$-\omega\psi_{11}$	$\omega^2\psi_{41}$	ψ_{21}	$\omega^2\psi_{31}$

3. Action of the PSG on low-energy eigenstates

Recall that the eigenstates of the low-energy excitations about the Fermi surface can be expressed in terms of eigenstates of the point-group rotation operators $8C_3$ [c.f. Eq. (47)].

Tables VI and VII list the action of the rotation elements of the PSG on these low-energy states. Since Eq. (47) is PT invariant, it is sufficient to consider the action of the rotation subgroup; the other PSG elements are combinations of rotations with the inversion, and cannot procure new information about the low-energy behavior. Note that proper rotations always map clockwise rotating states to clockwise states, and counter-clockwise to counter-clockwise. The improper rotations, conversely, map counter-clockwise rotating states into clockwise rotating states, and vice versa.

[1] P. W. Anderson, Mater. Res. Bull. **8**, 153 (1973).
[2] P. W. Anderson, Science **235**, 1196 (1987).
[3] C. Nayak, S. H. Simon, A. Stern, M. Freedman, and S. Das Sarma, Rev. Mod. Phys. **80**, 1083 (2008).
[4] R. Moessner, Can. J. Phys. **79**, 1283 (2001).
[5] A. P. Ramirez, Annu. Rev. Mater. Sci. **24**, 453 (1994).
[6] J. S. Helton *et al.*, Phys. Rev. Lett. **98**, 107204 (2007).
[7] R. Moessner and J. T. Chalker, Phys. Rev. B **58**, 12049 (1998).
[8] S. T. Bramwell and M. J. P. Gingras, Science **294**, 1495 (2001).
[9] C. Castelnovo, R. Moessner, and S. L. Sondhi, Nature (London) **451**, 42 (2008).
[10] U. Hizi and C. L. Henley, J. Phys.: Condens. Matter **19**, 145268 (2007).
[11] J. von Delft and C. L. Henley, Phys. Rev. Lett. **69**, 3236 (1992).
[12] O. Tchernyshyov, J. Phys.: Condens. Matter **16**, S709 (2004).
[13] A. B. Harris, A. J. Berlinsky, and C. Bruder, J. Appl. Phys. **69**, 5200 (1991).
[14] H. Tsunetsugu, Phys. Rev. B **65**, 024415 (2001).

[15] E. Berg, E. Altman, and A. Auerbach, Phys. Rev. Lett. **90**, 147204 (2003).
[16] R. Moessner, S. L. Sondhi, and M. O. Goerbig, Phys. Rev. B **73**, 094430 (2006).
[17] O. Tchernyshyov, R. Moessner, and S. L. Sondhi, Europhys. Lett. **73**, 278 (2006).
[18] G. Baskaran, Z. Zou, and P. W. Anderson, Solid State Commun. **63**, 973 (1987).
[19] J. B. Marston and I. Affleck, Phys. Rev. B **39**, 11538 (1989).
[20] V. Kalmeyer and R. B. Laughlin, Phys. Rev. Lett. **59**, 2095 (1987).
[21] X.-G. Wen, F. Wilczek, and A. Zee, Phys. Rev. B **39**, 11413 (1989).
[22] S. Chakravarty, Ph.D. thesis, Princeton University, 2006.
[23] R. Shankar, F. J. Burnell, and S. L. Sondhi, Ann. Phys. (N.Y.) **324**, 267 (2009).
[24] X.-G. Wen, Phys. Rev. B **65**, 165113 (2002).
[25] F. J. Burnell and S. L. Sondhi (to be published).
[26] J. H. Kim and J. H. Han, Phys. Rev. B **78**, 180410(R) (2008).
[27] M. Hermele, T. Senthil, M. P. A. Fisher, P. A. Lee, N. Nagaosa, and X.-G. Wen, Phys. Rev. B **70**, 214437 (2004).
[28] I. Affleck, Z. Zou, T. Hsu, and P. W. Anderson, Phys. Rev. B **38**, 745 (1988).
[29] E. Dagotto, E. Fradkin, and A. Moreo, Phys. Rev. B **38**, 2926 (1988).
[30] D. S. Rokhsar, Phys. Rev. B **42**, 2526 (1990).
[31] D. S. Rokhsar, Phys. Rev. Lett. **65**, 1506 (1990).
[32] C. Gros, Ann. Phys. (N.Y.) **189**, 53 (1989).
[33] Y. Ran, M. Hermele, P. A. Lee, and X.-G. Wen, Phys. Rev. Lett. **98**, 117205 (2007).
[34] J.-B. Fouet, M. Mambrini, P. Sindzingre, and C. Lhuillier, Phys. Rev. B **67**, 054411 (2003).
[35] X.-G. Wen, Phys. Rev. Lett. **88**, 011602 (2001).
[36] M. Hermele, T. Senthil, and M. P. A. Fisher, Phys. Rev. B **72**, 104404 (2005).
[37] D. Ceperley, G. V. Chester, and M. H. Kalos, Phys. Rev. B **16**, 3081 (1977).
[38] G. Misguich, *Quantum Spin Liquids*, Lecture Notes of the Les Houches Summer School 2008 (unpublished).
[39] G. Misguich and C. Lhuillier, *Two-Dimensional Quantum Antiferromagnets*, edited by H. T. Diep, Frustrated Spin Systems (World Scientific, Singapore, 2005), p. 981.
[40] H. Nielsen and M. Ninomiya, Nucl. Phys. B **185**, 20 (1981).
[41] For an introduction to this area see the recent Les Houches lectures by Misguich (Ref. 38) and the older review article (Ref. 39).
[42] Here we use the term "topological phases" in the looser sense of any phase with emergent gauge fields. Strictly speaking the term should be reserved for cases where the low-energy gauge theory is a purely topological gauge theory.
[43] This is as good a place as any to note that there is not, to date, a good experimental $S=1/2$ antiferromagnet on the pyrochlore lattice.
[44] Reference 17 shows that at asymptotically small boson densities the system *must* break some symmetry. The minor caveat is that this does not rule out a different solution intervening right near $S=1/2$.
[45] We are grateful to Michael Hermele for emphasizing this point.
[46] This Fermi surface does not display fermion doubling in the naive sense; all four bands cross at only one point in the Brillouin zone. This does not violate the result of Ref. 40, which assumes that levels are degenerate only at a finite set of points.
[47] See Refs. 27 and 36, and references therein.